Available online at www.sciencedirect.com
SCIENCE DIRECT®
Journal of Non-Crystalline Solids 348 (2004) 30–37
JOURNAL OF NON-CRYSTALLINE SOLIDS
www.elsevier.com/locate/jnoncrysol

Synthesis and characterization of niobium phosphate glasses containing barium and potassium

F.F. Sene, J.R. Martinelli *, L. Gomes

Energy and Nuclear Research Institute, Center of Materials Science and Technology, Av. Lineu Prestes, 2242, Cidade Universitária, CEP 05588-900 Sao Paulo, SP, Brazil

Abstract

The structural characteristics of phosphate glasses containing different amounts of Nb were investigated by X-ray diffraction, thermal analysis, Raman, and infrared spectroscopy. Phosphate glasses can be produced with relatively high amount of niobium by increasing the cooling rate without crystallization. Niobium is a glass former, is located in octahedral sites, and replaces tetrahedral phosphate groups by P, Nb, and O linked mixed chains. The density increases from 3.32 g/cm^3 to 3.73 g/cm^3, the elastic modulus increases from 56 GPa to 78 GPa, and the linear thermal expansion coefficient decreases from $24.7 \times 10^{-6}\,°C^{-1}$ to $7.9 \times 10^{-6}\,°C^{-1}$ as the amount of Nb increases. The glass transition temperature (T_g) increases from 480 °C to 653 °C as the amount of Nb increases from 5 to 37 mol% because the Nb–O–P and Nb–O–Nb linkages are stronger than the O–P bond, requiring higher temperatures for relaxation. Electrical measurements showed that the activation energy for ionic conduction increases from 0.46 eV to 0.59 eV for glasses containing 19–32 mol% of Nb_2O_5.

1. Introduction

Niobium phosphate glasses have been investigated because they might be used in a wide range of applications, such as wasteform for radioactive waste immobilization [1], rare-earth ion hosts for laser glasses [2], glass fibers and optical lenses [3,4], hermetic sealing [5], electrodes [6], and agricultural applications [7]. Besides that, phosphate glasses are easy to produce at relatively low temperatures (900–1200 °C).

Previously reported high performance liquid chromatography, HPLC [8], Fourier transformed infrared spectroscopy, FTIR [9], and Raman spectroscopy [10] data showed that phosphate glasses consist of a sequence of $[PO_4]^{3-}$ tetrahedrons formed by one phosphorous atom in the center and four oxygen atoms in the corner. Three of these oxygen atoms are known as bridging oxygen because they link three $[PO_4]^{3-}$ units. The other oxygen has a double bound with the phosphorous atom in the $[PO_4]^{3-}$ unit. A single $[PO_4]^{3-}$ unit can be linked to three other ones by –P–O–P– linkages, as observed in crystalline P_2O_5, however, with different bending angles. This structure is known as polyphosphate chains. The addition of cations, such as Ca^{2+}, depolymerizes the three-dimensional network, by breaking the –P–O–P– bonds, leading to non-bridging oxygen ($–P–O^-$). In this case, $[PO_4]^{3-}$ tetrahedrons form a bi-dimensional network.

The size of the polymeric chains decreases as the amount of modifiers increases, easing the formation of terminal groups $[PO_3]^-$ due to the bound breakage between the $[PO_4]^{3-}$ tetrahedrons. However, by increasing the amount of metallic cations, the tendency for crystallization also increases.

* Corresponding author.
E-mail address: jroberto@ipen.br (J.R. Martinelli).

0022-3093/$ - see front matter © 2004 Elsevier B.V. All rights reserved.
doi:10.1016/j.jnoncrysol.2004.08.122

Niobium phosphate glasses were previously investigated [11] to obtain chemical resistant materials with optical transparency. Several compositions were prepared by melting inorganic precursors in an induction furnace [11]. However, in all previously studied compositions, PbO was added as a glass modifier; these glasses are very stable, and chemically resistant [11]. These characteristics were associated with the O–Nb–O bonds. Further studies using FTIR showed that Nb^{5+} replaces P^{5+} in tetrahedral coordination in the P–O–P bonds. The bridging oxygen is now bonded to Nb^{5+}, forming O–P–O–Nb–O– type chains. It was also shown [12] that P–O type bonds are mostly found in terminal sites of the chain, while Nb–O bonds are located in the middle of the chains [12]. The Raman bands were assigned to O–Nb–O, O–P–O, and mixed O–P–O–Nb–O– chains (named PNb). As the amount of Nb_2O_5 increases, the larger will be the number of Nb–O–Nb and PNb bonds.

From the nuclear magnetic resonance spectroscopy (NMR) data [11] it was concluded that the number of Q^2 and Q^3 is relatively small and, as the amount of niobium increases, O–P–O bonds are replaced by PNb. Niobium is in octahedral coordination.

In the present work, niobium phosphate glasses containing barium and potassium were produced at different cooling rates, and characterized by X-ray diffraction, Raman spectroscopy, and FTIR spectroscopy, to verify the composition range of glass formation, and to provide a structural characterization. The hardness, density, modulus of elasticity, and electrical resistivity were also measured as a function of Nb_2O_5 concentration, as a complementary characterization of these glasses.

2. Experimental procedure

2.1. Glass preparation

Glasses were prepared by mixing different amounts of $(NH_4)_2HPO_4$, Nb_2O_5, KOH, and $BaCO_3$. Two set of glasses were produced:

Set 1 – The molar ratio between phosphorous pentoxide, barium oxide, and potassium oxide were kept constant: $[P_2O_5] = 1/2$ and $[BaO] = [K_2O] = 1/4$; only the amount of Nb_2O_5 varied.

Set 2 – The molar ratio between phosphorous pentoxide, barium oxide and potassium oxide was kept constant: $[P_2O_5] = [BaO] = [K_2O] = 1/3$; only the amount of Nb_2O_5 varied.

Table 1 shows the batch composition for the materials produced in this work. The following code was used for sample identification: *y*-Nb-*x*, where *y* is the set number and *x* is the amount of Nb_2O_5 in mol%.

The batch was melted in an alumina crucible inside an electric furnace. The melting temperature ranged from 1250 °C to 1350 °C, depending on the composition. The liquid was maintained in air at that temperature for 90 min for homogenization, fining, and bubble removal. The liquid was cast into an aluminum mold from 480 °C to 550 °C to obtain samples varying in size from $10 \times 10 \times 10\,mm^3$ to $10 \times 10 \times 50\,mm^3$. By heating the mold, heterogeneous cooling, mechanical stresses, and cracks are avoided. Finally, the material was removed from the mold and annealed in the temperature range of 480–550 °C for 2 h in air, to release internal stresses.

Table 1
Nominal composition of materials (mol%)

Sample Code	$P_2O_5 + BaO + K_2O$	Nb_2O_5
1-Nb-0	100	0
1-Nb-5	95	5
1-Nb-10	90	10
1-Nb-14	86	14
1-Nb-19	81	19
1-Nb-26	74	26
1-Nb-32	68	32
1-Nb-37	63	37
1-Nb-40	60	40
1-Nb-45	55	45
1-Nb-50	50	50
1-Nb-60	40	60
2-Nb-0	100	0
2-Nb-5	95	5
2-Nb-10	90	10
2-Nb-14	86	14
2-Nb-19	81	19
2-Nb-26	74	26
2-Nb-32	68	32
2-Nb-37	63	37
2-Nb-40	60	40
2-Nb-45	55	45
2-Nb-50	50	50
2-Nb-60	40	60

2.2. Sample preparation

Glass bars were cut by using a low concentration diamond cutting disk at 1500 rpm, and 150 g as load. Slabs 1–4 mm in thickness were prepared. These slabs were ground over a commercial glass plate, using SiC particles from 600 mesh to 1000 mesh, washed in water and ultrasound, and polished using a polishing machine with alumina particles of 10–0.1 μm dispersed in water. Samples were washed in distilled water, using ultrasound, and finally dried.

2.3. Characterization

2.3.1. Differential thermal analysis

Differential thermal analysis was performed (Netzsch, model STA 490) to determine the glass transition

temperature (T_g), and the glass stability. Powder samples were prepared by grinding and sieving to select an average particle size of 10 μm. Samples were heated from room temperature to 900 °C at 10 °C/min.

2.3.2. X-ray diffraction

X-ray diffraction (*Rigaku*, model DMAX100, and Bruker, model D8) was used to determine the glass structure and its stability to crystallization, before and after heat treatments.

2.3.3. Dilatometry

Small glass rods 6 mm in diameter, 12 mm in length were prepared by cutting glass bars with diamond disks (*Isomet* model 2000) at 1500 rpm and 200 g load.

The glass transition temperature, softening point, working range, and linear thermal expansion coefficient were determined by dilatometric measurements (Netzsch, model 402). Samples were heated from room temperature to 750 °C at 6 °C/min in an air flow.

2.3.4. Raman spectroscopy

Raman spectroscopy was performed to help the identification of groups formed by glass formers and oxygen and the type of chain. A He–Ne ($\lambda_0 = 632.8$ nm) laser (Spectra Physics model 127), a detection system Charge Couple Device (CCD – Wright with resolution of 400×600 pixels), and a microscope (Olympus, model BH2-UMA) were used for these measurements.

2.3.5. Infrared spectroscopy

Fourier transform infrared spectroscopy (FTIR) was performed to identify groups formed by glass formers and modifiers, and the presence of hydroxyl radicals. Two types of samples were prepared: pellets and slabs. Pellets 12 mm in diameter and 0.5 mm in thickness, were prepared by mixing and pressing 2 wt% of glass powder (particle average size = 10 μm) with dehydrated KBr. Samples were kept at 110 °C before the analysis to avoid water absorption from the atmosphere.

2.3.6. Density

The glass density was determined by the Archimedes' method as a function of Nb_2O_5.

2.3.7. Electrical resistivity

Two probe dc electrical resistivity measurements were performed by using an electrometer (Keithley model 610C) from room temperature to 750 °C. The T_g and the activation energy (E_a) were determined as a function of Nb_2O_5 concentration. Colloidal silver was used as electrodes. A K-type thermocouple closed to the sample was used to monitor the temperature. All connecting wires were 0.5 mm platinum wires.

3. Results

3.1. X-ray diffraction

To determine the effects of the cooling rate in the glass formation, samples from set 1 and set 2 were cooled to room temperature at two different cooling rates.

Fig. 1 shows the X-ray diffraction patterns for samples produced from set 2 cooled at 18 °C/min. No crystalline phases for concentrations of Nb_2O_5 less than 26 mol% were observed. Samples produced by cooling the liquid at 35 °C/min show similar diffraction patterns, but no crystallization phases for Nb_2O_5 concentrations less than 45 mol% were observed. Therefore, niobium phosphate glasses can be produced with relatively large amount of niobium by increasing the cooling rate.

The crystalline phases for the sample 1-NB-32 after a heat treatment were identified by comparing the X-ray diffraction pattern shown in Fig. 2 with the JCPDS files as: β-$NbPO_5$, $NbOPO_4$, $Ba(PO_3)_2$, $BaNb_2O_6$, $K_4P_2O_7$, and K_3NbO_4.

3.2. Differential thermal analysis

The T_g's for samples of set 1 were determined from the DTA curves, and are shown in Table 2.

3.3. Density

Fig. 3 shows the densities of glasses as a function of the Nb_2O_5 concentration. A linear function was fitted to the data. The correlation coefficient of the fit was 0.98. The line was adjusted by the minimum square method.

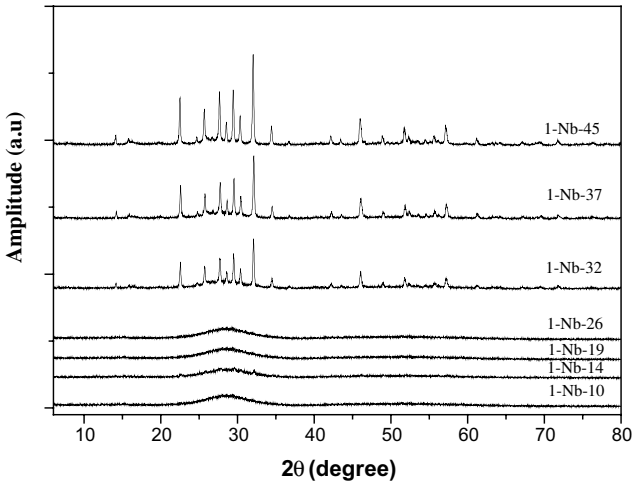

Fig. 1. X-ray diffraction patterns for samples of set 2 cooled at 18 °C/min.

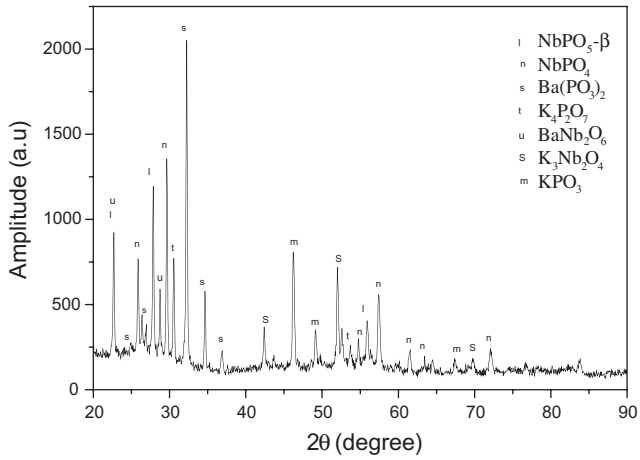

Fig. 2. X-ray diffraction patterns for 1-Nb-32 sample after a heat treatment.

Table 2
T_g as a function of Nb_2O_5 concentration

Nb_2O_5 concentration (mol%)	T_g (°C)
5	480 ± 5
14	554 ± 5
19	580 ± 5
26	601 ± 5
32	611 ± 5
37	653 ± 5

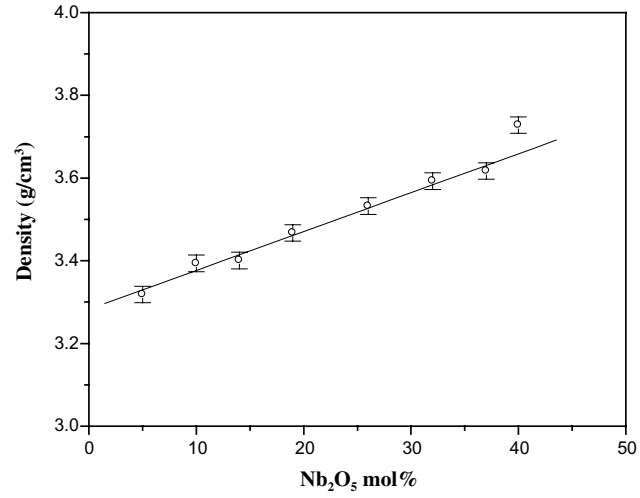

Fig. 3. Density as a function of Nb_2O_5 concentration.

3.4. FTIR

Fig. 4 shows the FTIR spectra for glasses with different amounts of Nb_2O_5.

3.5. Raman spectroscopy

Fig. 5 shows the Raman spectra for glasses of set 1.

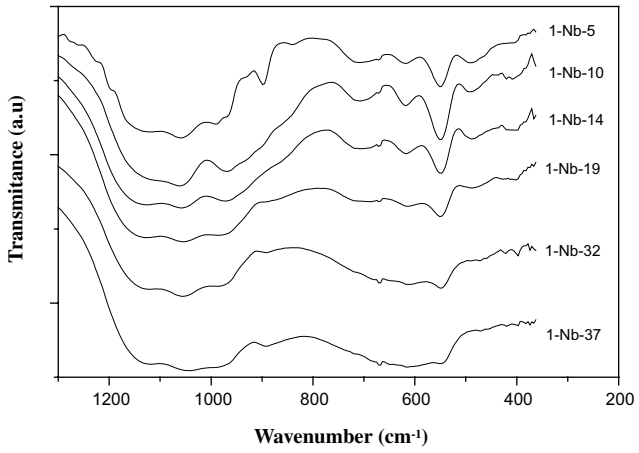

Fig. 4. FTIR spectra in the far infrared for niobium phosphate glasses.

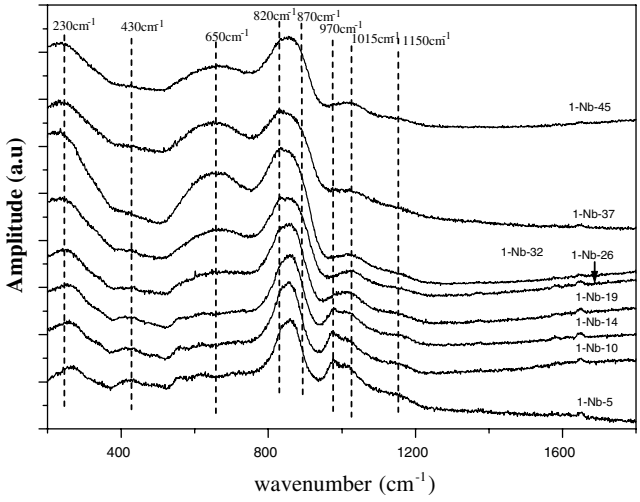

Fig. 5. Raman spectra for glasses of set 1.

3.6. Dilatometry

Table 3 shows the linear thermal expansion coefficient, α, the glass transition temperature, T_g, and the softening temperature, T_s, as a function of Nb_2O_5 concentration, determined from the dilatometric curves. As the amount of Nb_2O_5 increases, α decreases, T_g and T_s increase.

Table 3
Linear thermal expansion coefficient, T_g and T_s as a function of Nb_2O_5 concentration

Nb_2O_5 (mol%)	α (10^{-6} °C^{-1})	T_g (°C)	T_s (°C)
10	24.7 ± 0.5	510 ± 5	538 ± 5
19	10.2 ± 0.5	580 ± 5	647 ± 5
32	7.9 ± 0.5	609 ± 5	710 ± 5

3.7. Hardness

Fig. 6 shows the Vicker hardness of phosphate glasses as a function of Nb_2O_5 concentration.

3.8. Elastic modulus

Fig. 7 shows the elastic modulus of phosphate glasses as a function of Nb_2O_5 concentration.

3.9. Electrical resistivity

Fig. 8 shows the electrical resistivity as a function of the inverse of temperature. Arrhenius functions were fitted to the data for three glasses of set 1. The correlation coefficient for all curves is 0.99. The activation energies are 0.46 ± 0.02 eV, 0.51 ± 0.02 eV, and 0.59 ± 0.02 eV for glasses containing 19, 26, and 32 mol% of Nb_2O_5, respectively.

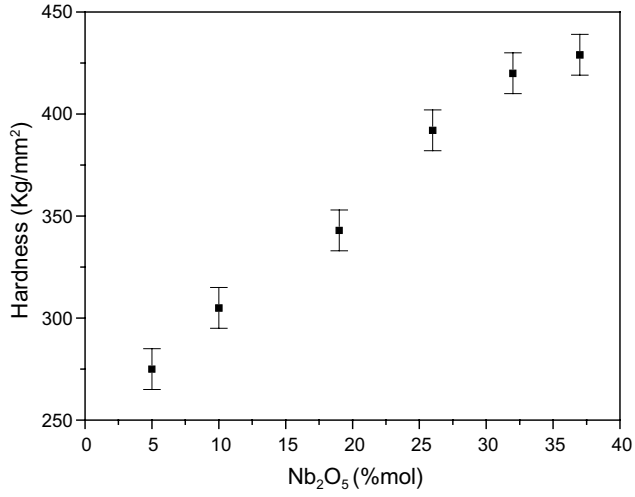

Fig. 6. Vickers hardness as a function of Nb_2O_5 concentration.

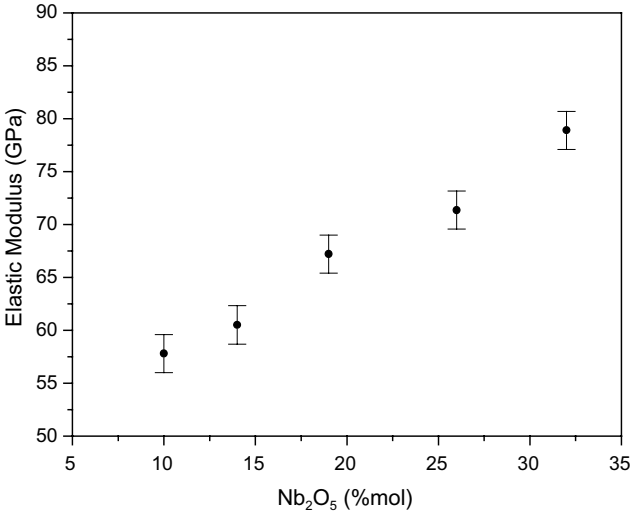

Fig. 7. Elastic modulus as a function of Nb_2O_5 concentration in phosphate glasses.

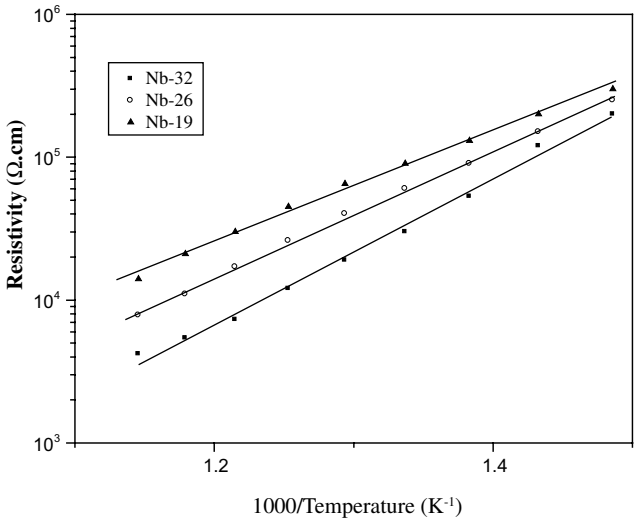

Fig. 8. Electrical resistivity as a function of inverse temperature in an Arrhenius type curve for glasses of set 1.

4. Discussion

4.1. Compositional diagrams

When cooling samples with composition of the set 1 group at 18 °C/min no crystalline phases are observed for amounts of Nb_2O_5 less than 40 mol%. The P mole fraction is larger for samples of set 1. Glasses containing just phosphorous as glass former and alkaline and alkaline earth modifiers are more stable, and in this case, when Nb is added, the probability to form P–O–P–O–P type chains and P–O–Nb–O–P–Nb mixed chains without crystallization is greater. Samples from set 1 can be produced with a relatively larger amount of Nb_2O_5 compared to set 2, without crystallization.

From the X-ray diffraction patterns two compositional diagrams were built for each cooling rate, as seen in Fig. 9 (cooling rate 18 °C/min) and Fig. 10 (35 °C/min).

From the thermal analysis data we noticed that T_g increases as the amount of Nb increases. The reason for that is that Nb–O–P and Nb–O–Nb linkages are stronger than the O–P bond, requiring higher temperatures for relaxation.

The stability of the glasses was evaluated by the Hruby parameter [13]:

$$H = (T_c - T_g)/(T_f - T_c), \quad (1)$$

where T_c is the temperature of maximum crystallization and T_f is the melting temperature for the crystallized

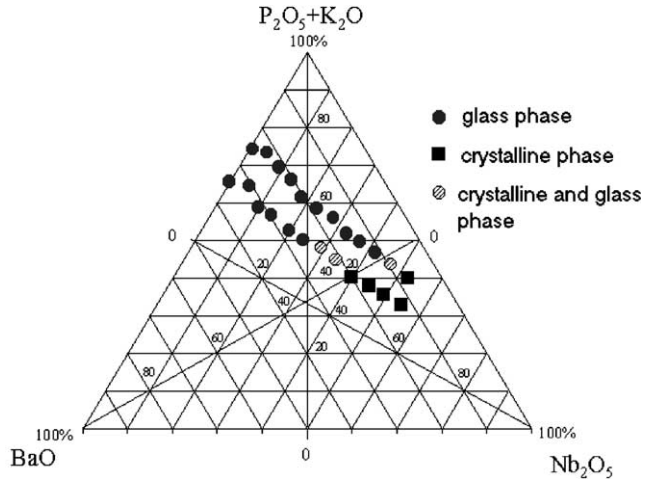

Fig. 9. Compositional diagram for samples cooled down at 18 °C/min.

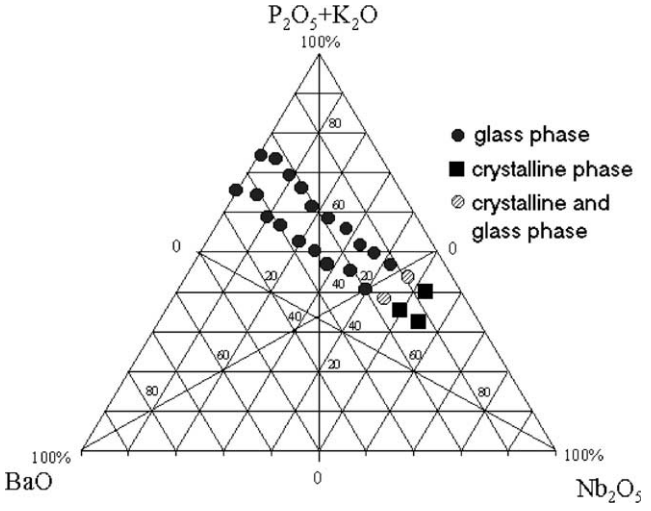

Fig. 10. Compositional diagram for samples cooled down at 35 °C/min.

sample. The Hruby parameter was larger than 1 for all glasses meaning that these glasses are stable concerning the crystallization.

As the amount of Nb_2O_5 increases, the density also increases as a linear function indicating that there are no abrupt changes in the glass structure affected by the addition of Nb_2O_5. For the sample with 45 mol%, crystalline phases were observed, so this fact explains why the experimental point is off the linear function in the density curve (Fig. 3).

The FTIR (Fig. 4) bands centered at 879 cm^{-1} and 702 cm^{-1} are assigned to asymmetric stretching and symmetric stretching vibrations of pyrophosphate groups (Q^1), respectively [14]. The band at 991 cm^{-1} is assigned to Q^0 $(PO_4)^{3-}$ groups [14]. The band centered at 1057 cm^{-1} is related to symmetric stretching vibrations of Q^2 (PO_2) groups [15]. The band centered at 490 cm^{-1} is related to a harmonic vibration assigned to bending of O–P–O and O=P–O bonds [16]. The tendency of the amplitude of the bands is to decrease as the amount of Nb_2O_5 increases. A band centered at 428 cm^{-1} was previously identified and assigned to O–Nb bonds [10]. The absorbance band centered at 540 cm^{-1} is related to a coupled mode including O–Nb bonds, vibration related to the bending of O–P–O bonds of $(PO_4)^{3-}$ groups [16] and coupled modes of O–Nb–O–P [15]. The intensity of this band increases as the amount of Nb_2O_5 increases in the range of 0–10 mol%, and decreases for larger amounts of Nb_2O_5, indicating that the intensity depends more on the groups with O–P bonds. Table 4 shows the tendency of the FTIR band amplitudes as the amount of Nb_2O_5 increases.

4.2. Raman spectroscopy

Raman absorption peaks related to Nb–O–Nb and Nb–O–P–O–Nb–O bonds are not very well resolved because of the typical broadening observed in amorphous structures. A deconvolution method was used to identify those peaks and to correlate them with the amount of Nb_2O_5. So, it is shown that the amplitude of the band at 820 cm^{-1} increases, the amplitude and the width of the band at 870 cm^{-1} decrease (Fig. 5) as the amount of Nb_2O_5 increases. These bands are assigned to bending modes of Nb–O–Nb bonds found in octahedral structures of NbO_6 and coupled bending modes of Nb–O–P–Nb–O and symmetrical stretching vibrations of Nb–O bonds found in NbO_6 octahedral groups [17]. The change of the intensity tendency as a function of the amount of Nb, for the bands at 820 cm^{-1} and 870 cm^{-1}, is related to the reduction of Nb–O–P–O groups and, consequently, the increase of Nb–O–Nb groups in the glass structure. The band at 230 cm^{-1} is related to the deformation modes of Nb–O–Nb bonds in octahedral NbO_6 groups, and also increases as the amount of Nb_2O_5 increases [15,17]. The band at 650 cm^{-1} is assigned to vibrations of Nb–O bonds [15,17] and its amplitude increases as the amount of

Table 4
Tendency of FTIR bands as a function of Nb_2O_5 concentration (s.s.v = symmetric stretching vibration, a.s.v = asymmetric stretching vibration, c.m = coupled modes, d.m = deformation modes)

Band (cm^{-1})	Assignment	Tendency of band intensity as the amount of Nb_2O_5 increases
428	c.m O–Nb and O–Nb–O–P	–
490	d.m O–P–O and O=P–O	Increases
540	O–Nb	Increases–decreases
702	s.s.v group Q^1	Increases
879	a.s.v group Q^2	Increases
991	Group Q^0 $(PO_4)^{3-}$	Increases
1057	s.s.v group Q^2	Increases

Nb_2O_5 increases. This band has been previously reported for α-$NbPO_5$ [17].

The bands at 970 cm^{-1} and 1015 cm^{-1} are assigned to asymmetric stretching of Q^0 $(PO_4)^{3-}$ groups and symmetric stretching of Q^1 $(PO_3)^{2-}$ groups [16], and their intensities decrease as the amount of Nb_2O_5 increases. A less pronounced shoulder at 1150 cm^{-1} is assigned to symmetric stretching vibrations of Q^2 (PO_2) chains [5]. As the amount of Nb_2O_5 increases, the amplitude of this shoulder decreases.

The band at 430 cm^{-1} is related to the coupled modes of O–Nb–O and O–P–O in similar systems [17]. The shoulder at 560 cm^{-1} is related to Q^n groups [18] and decreases as the amount of Nb_2O_5 increases.

Table 5 shows the amplitudes tendency of Raman bands as a function of Nb_2O_5 amount.

From the Raman and FTIR spectroscopy, we infer that niobium is a glass former in phosphate glasses since the addition of Nb leads to the formation of groups with O–Nb and O–P bounds. The tetrahedral coordinated groups, Q^n, are replaced by octahedral $[NbO_6]^{7-}$ with increasing Nb, and mixed structures are formed by O–P–O–Nb–O–Nb–O–P chains.

4.3. Dilatometry

According to the data shown in Table 3, as the amount of Nb_2O_5 increases, α decreases, T_g, and T_s increase. The thermal expansion coefficient (α) decreases because O–Nb bonds are stronger than O–P bonds [19], and the coordination number is larger. By increasing the concentration of Nb_2O_5 from 10 mol% to 19 mol%, α goes from $24.7 \pm 0.5 \times 10^{-6}\,°C^{-1}$ to $10.2 \pm 0.5 \times 10^{-6}\,°C^{-1}$. It seems that there is an inversely proportional dependence between α and Nb_2O_5 concentration. On the other hand, by varying the amount of Nb_2O_5 from 19% to 32%, α varies from $10.2 \pm 0.5 \times 10^{-6}\,°C^{-1}$ to $7.9 \pm 0.5 \times 10^{-6}\,°C^{-1}$.

Table 5
Tendency of Raman bands as a function of Nb_2O_5 (s.s.v = symmetric stretching vibration, a.s.v = asymmetric stretching vibration, c.m = coupled modes, d.m = deformation modes)

Band (cm^{-1})	Assignment	Tendency of band intensity as the amount of Nb_2O_5 increases
230	d.m Nb–O–Nb (NbO_6) octahedral	Increases
430	c.m O–Nb–O and O–P–O	Decreases
650	v.e Nb–O	Increases
820	d.m Nb–O–Nb (NbO_6) octahedral	Increases
870	c.m (s.s.v Nb–O–P) and Nb–O (short) in NbO_6	Decreases
970	s.s.v group Q^0	Decreases
1015	s.s.v group Q^1	Decreases
1150	s.s.v group Q^2	Decreases

For smaller concentrations of Nb_2O_5, we believe α is affected mainly by Nb bonds with other elements of the glass structure. By increasing the amount of Nb_2O_5, we believe the Nb ions take over other structural sites, including the formation of local ordered regions, which affects the variation of α.

4.4. Hardness

The hardness increases as the amount of Nb_2O_5 increases (Fig. 6). The Raman and FTIR spectroscopy data showed that structure groups with larger coordination are formed, and consequently, stronger bonds. This fact explains why α and the hardness increase as the amount of Nb_2O_5 increases.

4.5. Elastic modulus

The elastic modulus increases as the amount of Nb_2O_5 increases (Fig. 7). This fact can be explained by considering that the addition of Nb_2O_5 forms stronger and larger coordination structural groups, and the new structure is stronger and more resistant to deformation [20].

Niobium phosphate glasses have similar changes in these parameters with increasing Nb due to the existence of mixed structural groups formed by O–P and O–Nb bonds and octahedral coordinated NbO_6. The atoms that form these structural groups have a larger coordination number and the bond is stronger.

4.6. Electrical resistivity

The activation energy increases as a function of niobium concentration. The main conduction mechanism in this type of glass is ionic [21]. It was previously reported that V_2O_5 and Ta_2O_5 in phosphate glasses are responsible for an activation energy increase, decreasing the cation movement [21]. The T_g and the viscosity increase as V, Ta or Nb are added to phosphate glasses, consequently reducing the electrical conductivity and increasing the activation energy. It was also previously reported [21] that alkaline ion conduction in glass structure with octahedral coordinated groups is smaller than in glasses with only tetrahedral coordinated groups. Therefore, the results presented in Fig. 8 are in agreement with those observations, since the ionic conduction decreases as the amount of Nb_2O_5 increase, and the Nb is in an octahedral coordination.

5. Conclusions

Phosphate glasses were produced with an amount of niobium that was large when compared to previous studies [11] by increasing the cooling rate. Niobium is a glass former and replaces tetrahedral phosphate

groups by O–P–Nb–O–P–O and Nb–O–Nb chains in phosphate glasses.

The T_g increases as the amount of Nb increases because the Nb–O–P and Nb–O–Nb linkages are stronger than the O–P bond, requiring higher temperatures for relaxation.

The Hruby parameter was larger than 1 for all glasses indicating that these glasses are very stable concerning the crystallization.

As the amount of Nb_2O_5 increases, the density also increases as a linear function, so, there are no abrupt changes in the glass structure affected by the addition of Nb_2O_5.

The Raman and FTIR spectroscopy showed that structure groups with larger coordination are formed, and consequently, stronger bonds, explaining why the linear thermal expansion coefficient and the hardness increase as the amount of Nb_2O_5 increases.

The elastic modulus increases as the amount of Nb_2O_5 increases because the addition of Nb_2O_5 forms stronger and higher coordination structural groups, and the new structure is stronger and more resistant to deformation. The activation energy for ionic conduction increases as a function of niobium concentration.

Acknowledgments

The authors acknowledge Dr Dalva L.A. Faria (University of São Paulo – Chemistry Institute) for the Raman spectroscopy measurements, and MSc. Hiroshi Oikawa (Energy and Nuclear Research Institute) for the infrared spectroscopy measurements. The following funding agencies are also acknowledged: FAPESP Process no 96/9604-9 (XRD analyses), Fapesp Process no 99/08281-0, and CNPq (scholarship for F.F. Sene).

References

[1] B.C. Sales, L.A. Boatner, Lead–iron phosphate glass, in: W. Lutze, R.C. Ewing (Eds.), Radioactive Waste Forms for the Future, North-Holland Publ, 1988, p. 193.
[2] A.H. Khafagy, S.M. ElpRabaie, A.A. Higazy, A.S. Eid, Indian J. Phys. 74A (4) (2000) 433.
[3] B.C. Sales, L.A. Boatner, J. Am. Ceram. Soc. 70 (9) (1987) 615.
[4] W.S. Key, J.C. Miller, Phosphate glass for photonics, ORNL Rev. 27 (3) (1994) 12.
[5] I.W. Donald, J. Mater. Sci. 28 (1993) 2841.
[6] S.F. Anvari, C.A. Hogarth, G.R. Moridi, Electrical conductivity of zinc–barium phosphate glasses, J. Mater. Sci. 26 (1991) 3639.
[7] R. Pyare, L.J. Lal, V.C. Joshi, V.K. Singh, Leachability of molybdenum from ternary phosphate glasses, J. Am. Ceram. Soc. 79 (5) (1996) 1334.
[8] J.R. Van Vazer, Structure and properties of the condensed phosphates, J. Am. Chem. Soc. 72 (2) (1950) 639.
[9] K.P. Muller, Struktur und Eigeinschaften von Glasern und glasbildenden Schmelzen. Teil III, Glastechn. Ber. 42 (3) (1969) 83.
[10] R.K. Brow, T.M. Alam, D.R. Tallant, R.J. Kirkpatrick, M.R.S. Bull. (November) (1998) 63.
[11] N. Aranha, Vidros Niobofosfatos: Preparação, Caracterização e Propriedades, Tese de Doutorado, Unicamp, 1994.
[12] A. El Jazouli, J.C. Viala, C. Parent, G. Le Flem, P.H. Genmuller, J. Solid State Chem. 73 (1988) 433.
[13] A. Hruby, Czech. J. Phys. B-22 (1972) 1187.
[14] A. Rulmont et al., Eur. J. Solid Inorg. 40 (1980) 535.
[15] S.W. Martin, Eur. J. Solid Inorg. Chem. 28 (1) (1991) 163.
[16] C. Daynand, M.S. Graw, Structural investigations of phosphate glasses, J. Mater. Sci. 31 (1996) 1945.
[17] A. El Jazouli, R. Brochu, J.C. Viala, R. Ohazcuaga, C. Delmas, G. Le Flem, Ann. Chim. Fr. 7 (1982) 285.
[18] J.S. Andrade, A.G. Pinheiro, I.F. Vasconcelos, M.A.B. Araújo, M.A Valentee, A.S.B. Sombra, J. Phys. Chem. Solids 61 (2000) 899.
[19] R.C. Weast, M.J. Astle, CRC Handbook of Chemistry and Physics, CRC Press, Boca Raton, FL, USA, 1982.
[20] J.M.F. Navarro, El Vidreo, Consejo Superior de Investigaciones Científicas, Fundación Centro Nacional del Vidrio, Madrid, España, 1991.
[21] F. Pernot, R. Rogier, J. Mater. Sci. 28 (1993) 6676.